Misorientation-Controlled Cross-Plane Thermoelectricity in Twisted Bilayer Graphene

Phanibhusan S. Mahapatra,[1,*] Bhaskar Ghawri,[1,†] Manjari Garg,[2] Shinjan Mandal,[1] K. Watanabe,[3] T. Taniguchi,[3] Manish Jain,[1] Subroto Mukerjee,[1] and Arindam Ghosh[1,‡]

[1]*Department of Physics, Indian Institute of Science, Bangalore 560 012, India*

[2]*Department of Instrumentation and Applied Physics, Indian Institute of Science, Bangalore 560012, India*

[3]*National Institute for Materials Science, Namiki 1-1, Tsukuba, Ibaraki 305-0044, Japan*

(Received 17 September 2019; revised 8 May 2020; accepted 15 October 2020; published 24 November 2020)

The introduction of “twist” or relative rotation between two atomically thin van der Waals membranes gives rise to periodic moiré potential, leading to a substantial alteration of the band structure of the planar assembly. While most of the recent experiments primarily focus on the electronic-band hybridization by probing in-plane transport properties, here we report out-of-plane thermoelectric measurements across the van der Waals gap in twisted bilayer graphene, which exhibits an interplay of twist-dependent interlayer electronic and phononic hybridization. We show that at large twist angles, the thermopower is entirely driven by a novel phonon-drag effect at subnanometer scale, while the electronic component of the thermopower is recovered only when the misorientation between the layers is reduced to $< 6°$. Our experiment shows that cross-plane thermoelectricity at low angles is exceptionally sensitive to the nature of band dispersion and may provide fundamental insights into the coherence of electronic states in twisted bilayer graphene.

DOI: 10.1103/PhysRevLett.125.226802

The van der Waals (vdW) interaction between two graphene membranes in a moiré superlattice [Fig. 1(a)] can be precisely manipulated by a relative rotation or twist between the constituent layers [1–10]. At a small twist angle, the strong interlayer hybridization can alter the low-energy superlattice band structure significantly, leading to a phase-coherent tunneling of electrons across the layers with a renormalized Fermi velocity [9,11–14]. The phase coherence of the interlayer tunneling is maintained as long as the tunneling timescale ($\hbar/\gamma$, where γ is the interlayer coupling) is smaller than the in-plane dephasing timescale (τ) [8]. In contrast, the interlayer hybridization for a large twist angle occurs at higher energies and hence at higher doping, leaving the low-energy bands of the two layers essentially decoupled at low temperature (T). As a result, electrons tunnel incoherently across the vdW gap as the two successive tunneling events no longer remain phase coherent ($\hbar/\gamma \gg \tau$) [6,8,12]. However, at the temperature scale set by the Bloch–Grüneisen temperature, $T > T_{\mathrm{BG}} = 2\hbar v_{\mathrm{ph}} k_F/k_B$, where k_B, v_{ph}, and k_F are the Boltzmann constant, phonon velocity, and Fermi wave vector, respectively, the low-energy quasiparticle excitations are coupled with the layer breathing mode (LBM) of phonons through electron-phonon (e-ph) scattering [5,15]. The phonon-mediated recoupling of the two layers manifests in an unconventional phonon-drag effect in the thermoelectric transport between two atomically thin layers [15]. This completely phonon-driven thermoelectric transport persists even at low temperatures, suggesting that the electric and thermoelectric transport coefficients cannot be related by the semiclassical Mott relation for conventional tunnel junctions [15,16] or single layer graphene (SLG) [17,18]. Recent investigations suggest ultralow phonon conductance at the vdW interface between the graphene

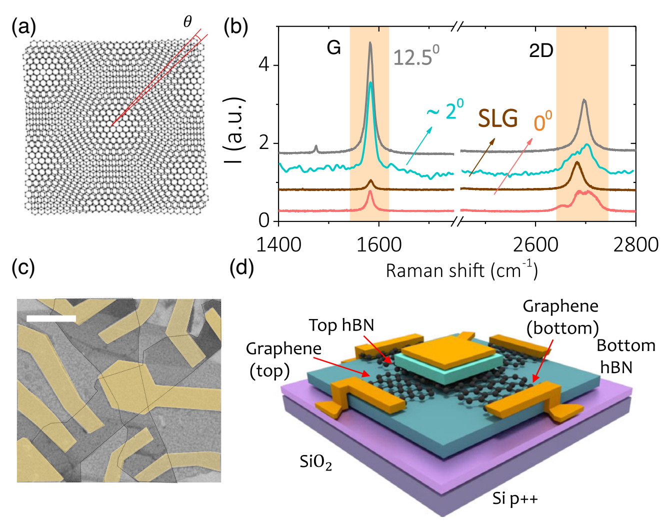

FIG. 1. Device structure and characterization. (a) Moiré superlattice when a relative rotation (θ) is introduced between two graphene layers. (b) The Raman spectra for G peak and 2D peak (shaded region) are compared for $\theta \sim 12.5°$, $\theta \sim 2°$, $\theta = 0°$, and single layer graphene with relative offset in the intensity for clarity. (c) SEM image of a device with twist angle $\theta = 0°$ (Bernal stacking). The scale bar represents a length of 5 μm. (d) Device schematic for the cross-plane electrical and thermoelectric measurements.

sheets [19] and other nanomaterials [20,21], resulting in significant enhancement of the thermoelectric figure of merit (*ZT* factor) [22]. However, the relevance of layer-hybridized phonons in the thermoelectric transport remains unclear when the electronic hybridization of the two layers becomes strong at low θ. A systematic experimental study on twist angle dependence is needed to develop the physics of the interlayer energy transport when the vdW interface is subjected to a statistical driving force by establishing a temperature gradient.

In this Letter, we report the measurement of thermoelectric transport across a single vdW gap formed in twisted bilayer graphene (tBLG). To have independent access to both layers as well as the cross junction, we create the vdW stack of two graphene layers at $60° + \theta$, where θ is the specific misorientation angle. The graphene superlattice is then encapsulated within two hexagonal boron nitride layers in a vertical stack on Si-SiO_2 substrate [see Fig. 1(d)]. We have measured a total of seven devices, four with large twist angles, one with Bernal-AB stacking ($\theta = 0°$), and two with the small twist angles $\theta \sim 2°$ and $\sim 4°$. The observed difference in the Raman spectra from the monolayer graphene and overlap region [Fig. 1(b)] suggests the twist angles $\theta \sim 6°$, 10°, 12.5°, and 14° for the devices with large θ [see Section II of the Supplemental Material (SM) [23] for more details]. The doped Si-SiO_2 substrate acts as a global bottom gate, while a local top gate on the overlap region controls the doping density (n) of the overlap region independently as shown in the SEM image in Fig. 1(c).

Figure 2(a) depicts the measurement schematic for the four-terminal cross-plane conductance (G_{cp}). In order to avoid the artifacts arising from asymmetric coupling of the voltage leads to the current path in a cross four-probe geometry [29], we perform quasi-four-probe measurements of the cross-plane resistance (R_{cp}) where current and voltage leads of the same polarity were placed on the same branch of the crossed structure. The high back-gate potential ($|V_{bg}| > 30$ V) ensures that the series resistance from outside the top-gated region is not more than ~5%–20% of R_{cp}, being dependent on doping and the lead configuration [see Fig. 2(b) and SM Sections III–VI [23] for more details]. The cross-plane charge transport can be driven by two distinct processes: (1) interlayer charge tunneling and (2) phonon-assisted charge transfer [5,6,15]. For large θ, the interlayer conduction at low temperature ($T \lesssim 70$ K) originates from incoherent tunneling between the two graphene layers, leading to a temperature-independent G_{cp} [6,8]. However, at higher temperature, the LBM phonons assist in interlayer conduction through e-ph scattering, leading to an increasing G_{cp} with temperatures as shown in Fig. 2(c) for $\theta \sim 12.5°$ [5,6,15]. The T dependence of cross-plane conductance in low twist angles is distinctly different from that at large θ, since G_{cp} is almost temperature independent, as shown for $\theta \sim 2°$ in Fig. 2(d). The T independence of G_{cp} is consistent

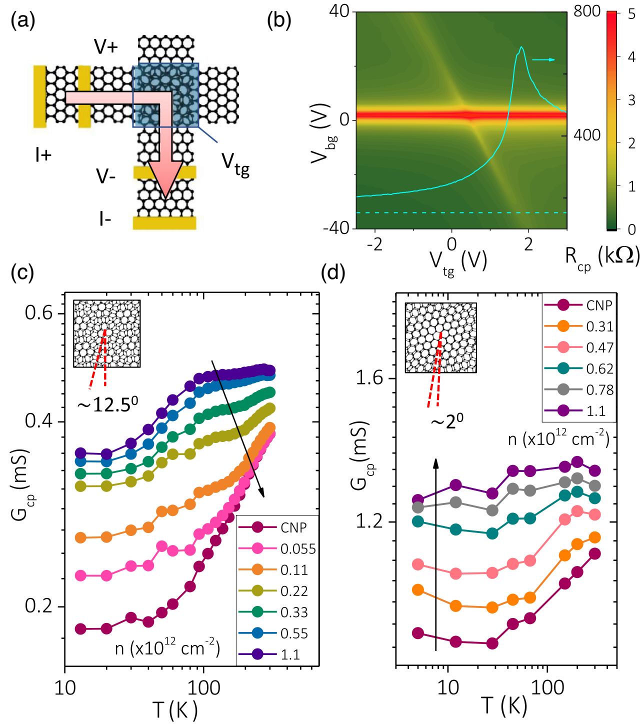

FIG. 2. Cross-plane electrical transport. (a) Schematic for the four-terminal cross-plane conductance measurements. (b) The cross-plane resistance (R_{cp}) as a function of top-gate (V_{tg}) and bottom-gate (V_{bg}) potentials for $\theta \sim 4°$. R_{cp} as a function of V_{tg} is shown by cyan curve from a line cut at fixed $V_{bg} = -34$ V (dotted line). Temperature dependence of G_{cp} for (c) $\theta \sim 12.5°$ and (d) $\theta \sim 2°$, respectively, for different values of carrier density (n) measured from the charge neutrality point (CNP).

across all low θ devices, indicating the absence of phonon-mediated scattering in cross-plane conduction when the two layers are strongly hybridized (see SM Section VII [23]).

The cross-plane thermoelectric power (TEP) or Seebeck coefficient is obtained from $S(V_{tg}, T) = V_{2\omega}/\Delta T$, where ΔT is the effective temperature difference between the two graphene layers, created by passing a sinusoidal heating current (I_ω) in the top graphene layer [Fig. 3(a)]. The resulting second harmonic thermovoltage $V_{2\omega}$ is recorded between the two layers for various top-gate-induced doping, while the back gate is set at a high potential to minimize the in-plane contributions in $V_{2\omega}$ [Fig. 3(b)] [15,17]. The cross-plane ΔT is measured using resistance thermometry of the top graphene layer (see SM Section IX [23]). For the range of heating current used, $I_\omega \sim 1$–$4\ \mu$A, both $V_{2\omega}$, $\Delta T \propto I_\omega^2$ [Fig. 3(c)] ensure that the measurements were performed within the linear response regime ($\Delta T \ll T$) [30] and the Seebeck coefficient S is independent of the ΔT itself.

First, we compare the temperature dependence of S at various carrier densities for $\theta \sim 12.5°$ in Fig. 3(d). The measured S exhibits a nonlinear T dependence as observed

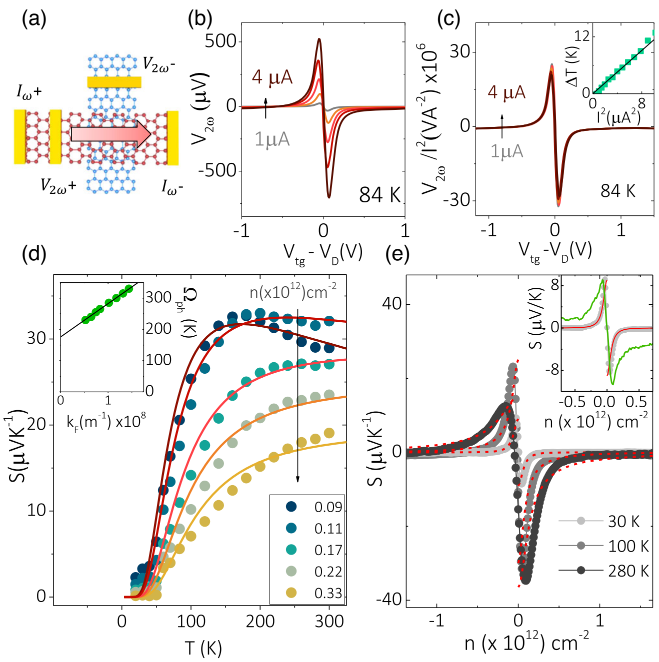

FIG. 3. Thermoelectric transport at large twist angle ($\theta \sim 12.5°$). (a) In-plane heating and measurement scheme for cross-plane thermovoltage $V_{2\omega}$. (b) $V_{2\omega}$ with varying top-gate voltages $|V_{tg} - V_D|$ for different in-plane heating currents (1–4 μA) at 84 K. (c) $V_{2\omega}$ normalized with I_ω^2. The inset shows that the measured temperature difference $\Delta T \propto I_\omega^2$. (d) Temperature dependence of $S = V_{2\omega}/\Delta T$ for $\theta \sim 12.5°$ device for various n. The solid lines show the fit of the TEP described in Eq. (1). The inset shows the obtained phonon energy as a function of Fermi wave vector k_F. (e) The density dependence of the measured S for three representative temperatures (circles). The dashed lines show the fitted S from the phonon-drag TEP [Eq. (1)]. The inset shows the comparison between the measured S (gray line) and the calculated S (green line) from the Mott relation [Eq. (2)] at $T = 30$ K. The red lines show the fit of the phonon-drag-mediated TEP.

in our previous work [15], which suggests that the cross-plane TEP is primarily driven by the interlayer phonons. A phonon-driven TEP involves a temperature difference (ΔT)-induced quasi-nonequilibrium condition that leads to net diffusion of phonons from the hot layer to the cold layer. These out-of-equilibrium phonons then impart momentum to the charge carriers through e-ph scattering, leading to a frictional drag force [31,32] on the charge carriers. In the steady state, this phonon-drag force results in additional thermal voltage between the two layers due to the interlayer charge imbalance. For the quadratic dispersion relation of LBM branch of phonons [5,15], the phonon-drag component of TEP can be expressed as [31]

$$S \approx \frac{\alpha\Omega_{\rm ph}}{neT^2}\frac{e^{\Omega_{\rm ph}/T}}{(e^{\Omega_{\rm ph}/T}-1)^2}, \qquad (1)$$

where n is the number density of the carriers with charge e and the prefactor α captures different phonon scattering rates. Here $\Omega_{\rm ph}(\boldsymbol{q}_K, k_F)$ is the energy of the LBM phonon that elastically scatters one electron from the Fermi circle of (k_F) one layer to another that is separated by momentum $\boldsymbol{q}_K$ (for more details, see SM Section X [23]).

The phonon-drag-mediated TEP in Eq. (1) shows excellent fit to the T dependence of S at various doping densities for $\theta \sim 12.5°$, as shown in Fig. 3(d). The fitting parameter α is found to be temperature independent for higher doping but becomes weakly temperature dependent $\sim T^{-\gamma}$, where $\gamma \approx 0.1$–0.3, close to CNP. The fit of Eq. (1) to the T dependence of TEP yields $\Omega_{\rm ph}(\boldsymbol{q}_K, k_F) \sim 200$–$300$ K and exhibits linear dependence on the Fermi wave vector k_F [inset Fig. 3(d)]. This is the direct consequence of momentum conservation in the interlayer e-ph scattering as the average phonon momentum required to scatter one electron from one layer to another $\approx \boldsymbol{q}_K + k_F$ [15]. The intercept $\Omega_{\rm ph}(\boldsymbol{q}_K, k_F = 0) \approx 175$ K coincides well with the low-energy LBM branch $\mathrm{ZO}'/\mathrm{ZA}_2$ in tBLG [15,33,34].

The density dependence of S, shown in Fig. 3(e) (red dotted lines) for three different temperatures, can also be obtained quantitatively from a electron-phonon scattering scenario. In fitting the phonon-drag TEP, we have used Eq. (1) and the linear dependence of $\Omega_{\rm ph}$ on $k_F = \sqrt{\pi n}$ with a charge-puddle broadening factor (n_0) in the density n such that $\Omega_{\rm ph} = \Omega_0 + \beta\sqrt{\pi(n_0^2 + n^2)^{\frac{1}{2}}}$, where the coefficients Ω_0 and β are taken from the linearity of $\Omega_{\rm ph}$ on k_F.

In contrast to the large θ devices, TEP in low twist angle ($\theta < 6°$) devices [Fig. 4(a),(b)] exhibits a linear dependence on temperature throughout the experimental temperature range (∼30–300 K). This is qualitatively similar to the Mott thermopower ($\sim T/T_F$) observed for graphene in-plane and diffusive conductors in the degenerate limit $k_B T \ll \mu$, where μ is the chemical potential [17,35] but differs from in-plane TEP in graphite [36]. While the origin of TEP $\propto T$ can be attributed to the interlayer entropy transport by the thermally activated quasiparticles over the Fermi energy, the absence of nonlinearity in T dependence of S also indicates that the phonon-drag effects are negligible in low twist angles irrespective of T.

We now analyze the doping dependence of S in both $\theta \sim 2°$ and $\theta = 0°$ devices considering that the TEP is composed of the electronic component and hence determined by the Mott relation [17,37],

$$S_{\rm Mott} = -\frac{\pi^2 k_B^2 T}{3|e|}\frac{1}{G_{\rm cp}}\frac{dG_{\rm cp}}{dV_{\rm tg}}\frac{dV_{\rm tg}}{dE}\bigg|_{E=E_F}. \qquad (2)$$

$S_{\rm Mott}$ in Eq. (2) can be evaluated by differentiating the experimentally measured $G_{\rm cp}$ with respect to $V_{\rm tg}$ and using the parallel plate model of gate capacitance. For $\theta \sim 2°$, the Dirac dispersion of SLG, $E_F = \hbar v_F\sqrt{\pi n}$, yields $(dV_{\rm tg}/dE) = (2/\hbar v_F)\sqrt{(2e/\pi C_{\rm BN})|V_{\rm tg} - V_D|}$, where $v_F = 10^6$ ms^{-1} and $C_{\rm BN}$ are the Fermi velocity in the SLG and gate capacitance per unit area, respectively. In

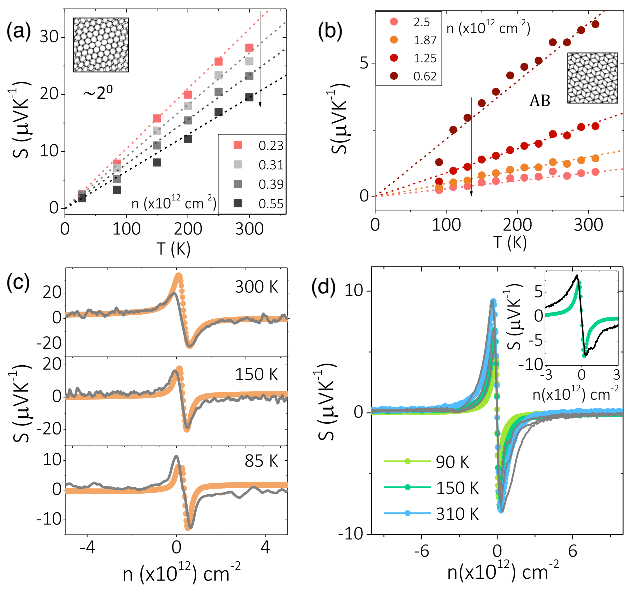

FIG. 4. Cross-plane thermoelectricity at low twist angle. Temperature dependence of S for (a) $\theta \sim 2°$ and (b) $\theta = 0°$ (Bernal stacking) for various n. The dashed lines show the linear T behavior as a guide for the eye. The doping dependence of experimentally measured S (colored circles) is compared to S_{Mott} (gray solid lines) for (c) $\theta \sim 2°$ and (d) $\theta = 0°$ at various temperatures. S_{Mott} is calculated using the (c) single layer Dirac dispersion and (d) parabolic band dispersion of bilayer graphene. The inset in (d) shows the density dependence of S for $\theta = 0°$ compared to that of normalized S_{Mott} (black line) evaluated from the single layer Dirac dispersion at a fixed representative temperature $T = 150$ K.

calculating dV_{tg}/dE, we have assumed that the gate potential $|V_{\mathrm{tg}} - V_D|$ induces equal doping density in both layers due to negligible screening of electric field from the graphene sheet and small interlayer separation $d \sim 0.34$ nm [6,38,39] (see SM Section XIV [23] for discussion on the effect of screening on interlayer charge imbalance and Seebeck coefficient). We compare the doping dependence of TEP in $\theta \sim 2°$ with Mott relation at various temperatures in Fig. 4(c). S_{Mott} obtained from Eq. (2) coincides well with the measured S for the three representative temperatures. The quantitative agreement of S with S_{Mott} also suggests that the renormalization effects on v_F due to the flattening of the lowest-energy bands are not significant in our device [12].

For a Bernal stacked tBLG device, S_{Mott} is evaluated by numerically differentiating the measured G_{cp} with respect to gate potential V_{tg} and using the parabolic dispersion of the bilayer graphene (BLG) [40,41],

$$E(k) = \frac{1}{2}\gamma_1\left[\sqrt{1 + \frac{v_F^2\hbar^2k^2}{\gamma_1^2}} - 1\right], \qquad (3)$$

where $\gamma_1 \approx 0.39$ eV is the interlayer hopping energy and $v_F \approx 0.95 \times 10^6$ is the Fermi velocity in the BLG. The BLG dispersion yields, $(dV_{\mathrm{tg}}/dE) = (4/\xi\gamma_1)\sqrt{1 + \xi|V_{\mathrm{tg}} - V_D|}$ where the factor $\xi = (4v_F^2\hbar^2\pi C_{\mathrm{BN}}/e\gamma_1^2) \approx 1$ for the gate dielectric (hexagonal boron nitride) of thickness ≈ 7 nm. An excellent quantitative agreement between the measured TEP and Mott relation was obtained [Fig. 4(d)] by scaling the S_{Mott} to compensate for the overestimation of the measured ΔT from resistive thermometry (see SM Section XII [23]). We verify that the similarly normalized S_{Mott}, when evaluated from the single layer Dirac dispersion, does not conform well with the density variation of measured S [inset of Fig. 4(d)]. This validates that the band dispersion is non-Dirac and parabolic in the hybridized overlap region, which suggests that the doping dependence of S is highly sensitive to the coherence of the electronic states via the band dispersion (see SM Section XIII [23]). Furthermore, we compare the electronic component of the TEP, S_{Mott}, to the measured S for a large twist angle, $\theta \sim 12.5°$, in the inset of Fig. 3(e) at low temperature (30 K). The observation of a large discrepancy from the Mott relation, even at low temperature ~ 30 K where $T/\Omega_{\mathrm{ph}} \ll 1$, strongly suggests that the purely electronic part of the TEP is absent at a large twist angle.

In Fig. 5(a), we present the T dependence of all devices at a fixed representative number density $n \sim 3 \times 10^{11}$ cm^{-2}, which is close to the CNP. We observe that the large twist angle devices ($\theta \sim 6°$–$14°$) show qualitatively similar nonmonotonic TEP, which is identified with the phonon-drag-mediated TEP. In contrast to large θ, the devices with a low twist angle ($\theta < 6°$) exhibit linear T dependence of S, indicating a crossover from phonon-driven thermoelectric transport to the purely coherent

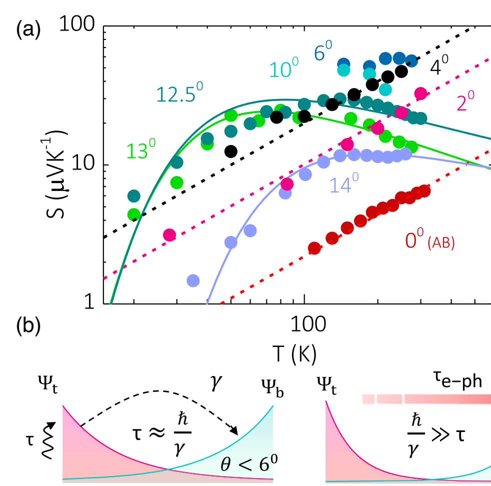

FIG. 5. Twist-controlled cross-plane thermoelectricity. (a) Seebeck coefficient as a function of temperature for seven different θ at a fixed doping of $n \sim 3 \times 10^{11}$ cm^{-2}. The solid lines show the fit of the phonon-driven TEP, while the dotted lines show the linear T dependence as a guide for the eye. The S-T data for $\theta \sim 13°$ are taken from Ref. [15]. (b) A schematic showing the interplay of the timescales associated with interlayer hybridization, dephasing, and electron-phonon scattering.

electronic transport. This striking shift of TEP from electronic hybridization to phononic hybridization with increasing twist angle demands further elaboration. We begin with estimating the generic e-ph scattering timescale $\tau_{\text{e-ph}}$ from the phonon energy Ω_{ph} obtained from the intercept in the Fig. 3(d) inset. As the interlayer e-ph scattering requires a phonon to be absorbed or emitted, the timescale $\tau_{\text{e-ph}} \sim \hbar/\Omega_{\text{ph}}$ can be estimated to be ~10 ps for $\Omega_{\text{ph}} \sim 100$ K. When the twist angle is reduced, $\tau_{\text{e-ph}}$ shows weak dependence on θ due to the quadratic dispersion of Ω_{ph}. However, when the twist angle is increased, the interlayer electronic tunneling timescale $\hbar/\gamma$ decays rapidly and becomes slower than $\tau_{\text{e-ph}}$ for $\theta > 6°$ [Fig. 5(b)] [8]. Consequently, e-ph scattering becomes the dominant mode of interlayer charge transport instead of the electronic tunneling at large θ. The observed phonon-drag TEP, even at $T \sim 30\ \text{K} \ll \Omega_{\text{ph}}$ when e-ph scattering is not expected to be dominant, is seemingly due to the e-ph scattering length becoming comparable to the mean free path or the cross-plane distance between the two layers, which is not unfamiliar in clean graphene samples [42]. However, when the mismatch is reduced to $\theta < 6°$, the strong interlayer hybridization drives the system to a coherent tunneling regime where the cross-plane tunneling timescale ($\hbar/\gamma \sim 10$–100 fs) is expected to be much faster [8] than the $\tau_{\text{e-ph}}$(~10 ps), effectively dominating any phonon contribution in the cross-plane transport and leading to $S \sim T/T_F$.

In summary, we have experimentally measured the cross-plane thermoelectricity across a single van der Waals gap between two rotated graphene layers with varying twist angles. The measured Seebeck coefficient exhibits unique dependence on the twist angle and hence on the hybridization of electronic and phononic bands of two graphene layers. At large twist angles, the cross-plane thermoelectric transport is entirely driven by the e-ph scattering from the hybridized phonons, which give rise to an unconventional phonon-drag effect at the subnanometer distance, while at low twist angles ($\theta < 6°$), the electronic hybridization is restored, resulting in a thermopower that can be described by the semiclassical Mott relation for coherent charge tunneling. The twist-controlled thermoelectricity can not only probe the interlayer coherent states in twisted bilayer graphene but may trigger new thermoelectric designs.

We thank H.R. Krishnamurthy, Tanmoy Das, and Sumilan Banerjee for valuable discussions. The authors thank DST for financial support and CeNSE (Centre for Nano Science and Engineering) for providing fabrication and characterization facilities. K. W. and T. T. acknowledge support from the Elemental Strategy Initiative conducted by the MEXT, Japan and the CREST (JPMJCR15F3), JST.

P. S. M. and B. G. contributed equally to this work.

[*]Corresponding author.
phanis@iisc.ac.in
[†]Corresponding author.
gbhaskar@iisc.ac.in
[‡]Also at Centre for Nano Science and Engineering, Indian Institute of Science, Bangalore 560 012, India.

[1] E. Koren, I. Leven, E. Lörtscher, A. Knoll, O. Hod, and U. Duerig, Coherent commensurate electronic states at the interface between misoriented graphene layers, Nat. Nanotechnol. **11**, 752 (2016).

[2] Y. Cao *et al.*, Correlated insulator behaviour at half-filling in magic-angle graphene superlattices, Nature (London) **556**, 80 (2018).

[3] Y. Cao, V. Fatemi, S. Fang, K. Watanabe, T. Taniguchi, E. Kaxiras, and P. Jarillo-Herrero, Unconventional superconductivity in magic-angle graphene superlattices, Nature (London) **556**, 43 (2018).

[4] E. Mele, Commensuration and interlayer coherence in twisted bilayer graphene, Phys. Rev. B **81**, 161405(R) (2010).

[5] V. Perebeinos, J. Tersoff, and P. Avouris, Phonon-Mediated Interlayer Conductance in Twisted Graphene Bilayers, Phys. Rev. Lett. **109**, 236604 (2012).

[6] Y. Kim *et al.*, Breakdown of the Interlayer Coherence in Twisted Bilayer Graphene, Phys. Rev. Lett. **110**, 096602 (2013).

[7] J. M. B. Lopes dos Santos, N. M. R. Peres, and A. H. Castro Neto, Graphene Bilayer with a Twist: Electronic Structure, Phys. Rev. Lett. **99**, 256802 (2007).

[8] R. Bistritzer and A. H. MacDonald, Transport between twisted graphene layers, Phys. Rev. B **81**, 245412 (2010).

[9] R. Bistritzer and A. H. MacDonald, Moiré bands in twisted double-layer graphene, Proc. Natl Acad. Sci. U.S.A. **108**, 12233 (2011).

[10] M. Yankowitz, S. Chen, H. Polshyn, Y. Zhang, K. Watanabe, T. Taniguchi, D. Graf, A. F. Young, and C. R. Dean, Tuning superconductivity in twisted bilayer graphene, Science **363**, 1059 (2019).

[11] S. Fang and E. Kaxiras, Electronic structure theory of weakly interacting bilayers, Phys. Rev. B **93**, 235153 (2016).

[12] A. Luican, G. Li, A. Reina, J. Kong, R. R. Nair, K. S. Novoselov, A. K. Geim, and E. Y. Andrei, Single-Layer Behavior and Its Breakdown in Twisted Graphene Layers, Phys. Rev. Lett. **106**, 126802 (2011).

[13] Y. Cao, J. Y. Luo, V. Fatemi, S. Fang, J. D. Sanchez-Yamagishi, K. Watanabe, T. Taniguchi, E. Kaxiras, and P. Jarillo-Herrero, Superlattice-Induced Insulating States and Valley-Protected Orbits in Twisted Bilayer Graphene, Phys. Rev. Lett. **117**, 116804 (2016).

[14] P. Moon and M. Koshino, Energy spectrum and quantum hall effect in twisted bilayer graphene, Phys. Rev. B **85**, 195458 (2012).

[15] P. S. Mahapatra, K. Sarkar, H. R. Krishnamurthy, S. Mukerjee, and A. Ghosh, Seebeck coefficient of a single van der Waals junction in twisted bilayer graphene, Nano Lett. **17**, 6822 (2017).

[16] H. Sadeghi, S. Sangtarash, and C. J. Lambert, Cross-plane enhanced thermoelectricity and phonon suppression in graphene/MoS_2 van der Waals heterostructures, 2D Mater. **4**, 015012 (2016).

[17] Y. M. Zuev, W. Chang, and P. Kim, Thermoelectric and Magnetothermoelectric Transport Measurements of Graphene, Phys. Rev. Lett. **102**, 096807 (2009).

[18] J. F. Sierra, I. Neumann, J. Cuppens, B. Raes, M. V. Costache, and S. O. Valenzuela, Thermoelectric spin voltage in graphene, Nat. Nanotechnol. **13**, 107 (2018).

[19] V. Hung Nguyen, M. C. Nguyen, H.-V. Nguyen, J. Saint-Martin, and P. Dollfus, Enhanced thermoelectric figure of merit in vertical graphene junctions, Appl. Phys. Lett. **105**, 133105 (2014).

[20] Y. Xiong *et al.*, Ultralow thermal conductance of the van der Waals interface between organic nanoribbons, Mater. Today Phys. **11**, 100139 (2019).

[21] W. Feng, X. Yu, Y. Wang, D. Ma, Z. Sun, C. Deng, and N. Yang, A cross-interface model for thermal transport across the interface between overlapped nanoribbons, Phys. Chem. Chem. Phys. **21**, 25072 (2019).

[22] Y. Anno, Y. Imakita, K. Takei, S. Akita, and T. Arie, Enhancement of graphene thermoelectric performance through defect engineering, 2D Mater. **4**, 025019 (2017).

[23] See Supplemental Material, which includes Refs. [24–28], at http://link.aps.org/supplemental/10.1103/PhysRevLett.125.226802 for more discussions on Raman spectroscopy, the cross-plane measurement technique, and interlayer screening.

[24] K. Kim, S. Coh, L. Z. Tan, W. Regan, J. M. Yuk, E. Chatterjee, M. F. Crommie, M. L. Cohen, S. G. Louie, and A. Zettl, Raman Spectroscopy Study of Rotated Double-Layer Graphene: Misorientation-Angle Dependence of Electronic Structure, Phys. Rev. Lett. **108**, 246103 (2012).

[25] V. Carozo, C. M. Almeida, E. H. M. Ferreira, L. G. Cançado, C. A. Achete, and A. Jorio, Raman signature of graphene superlattices, Nano Lett. **11**, 4527 (2011).

[26] R. W. Havener, H. Zhuang, L. Brown, R. G. Hennig, and J. Park, Angle-resolved Raman imaging of interlayer rotations and interactions in twisted bilayer graphene, Nano Lett. **12**, 3162 (2012).

[27] A. Riminucci, M. Prezioso, P. Graziosi, and C. Newby, Electrode artifacts in low resistance organic spin valves, Appl. Phys. Lett. **96**, 112505 (2010).

[28] T.-F. Chung, Y. Xu, and Y. P. Chen, Transport measurements in twisted bilayer graphene: Electron-phonon coupling and Landau level crossing, Phys. Rev. B **98**, 035425 (2018).

[29] J. M. Pomeroy and H. Grube, Negative resistance errors in four-point measurements of tunnel junctions and other crossed-wire devices, J. Appl. Phys. **105**, 094503 (2009).

[30] J. F. Sierra, I. Neumann, M. V. Costache, and S. O. Valenzuela, Hot-carrier seebeck effect: Diffusion and remote detection of hot carriers in graphene, Nano Lett. **15**, 4000 (2015).

[31] M. Wu, N. Horing, and H. Cui, Phonon-drag effects on thermoelectric power, Phys. Rev. B **54**, 5438 (1996).

[32] D. Cantrell and P. Butcher, A calculation of the phonon-drag contribution to the thermopower of quasi-2d electrons coupled to 3d phonons. i. General theory., J. Phys. C **20**, 1985 (1987).

[33] A. I. Cocemasov, D. L. Nika, and A. A. Balandin, Phonons in twisted bilayer graphene, Phys. Rev. B **88**, 035428 (2013).

[34] J. Campos-Delgado, L. G. Cançado, C. A. Achete, A. Jorio, and J.-P. Raskin, Raman scattering study of the phonon dispersion in twisted bilayer graphene, Nano Res. **6**, 269 (2013).

[35] E. H. Hwang, E. Rossi, and S. Das Sarma, Theory of thermopower in two-dimensional graphene, Phys. Rev. B **80**, 235415 (2009).

[36] C. Ayache, A. De Combarieu, and J. Jay-Gerin, Observation of a new anomaly in the low-temperature thermoelectric power of graphite: Interpretation by a phonon-drag effect acting on the h-point minority holes, Phys. Rev. B **21**, 2462 (1980).

[37] M. Jonson and G. Mahan, Mott's formula for the thermopower and the Wiedemann-Franz law, Phys. Rev. B **21**, 4223 (1980).

[38] J. D. Sanchez-Yamagishi, T. Taychatanapat, K. Watanabe, T. Taniguchi, A. Yacoby, and P. Jarillo-Herrero, Quantum Hall Effect, Screening, and Layer-Polarized Insulating States in Twisted Bilayer Graphene, Phys. Rev. Lett. **108**, 076601 (2012).

[39] L. Britnell *et al.*, Field-effect tunneling transistor based on vertical graphene heterostructures, Science **335**, 947 (2012).

[40] E. McCann, Asymmetry gap in the electronic band structure of bilayer graphene, Phys. Rev. B **74**, 161403(R) (2006).

[41] S.-G. Nam, D.-K. Ki, and H.-J. Lee, Thermoelectric transport of massive dirac fermions in bilayer graphene, Phys. Rev. B **82**, 245416 (2010).

[42] F. Ghahari, H.-Y. Xie, T. Taniguchi, K. Watanabe, M. S. Foster, and P. Kim, Enhanced Thermoelectric Power in Graphene: Violation of the Mott Relation by Inelastic Scattering, Phys. Rev. Lett. **116**, 136802 (2016).